TOPICAL REVIEW — MAGNETISM, MAGNETIC MATERIALS, AND INTERDISCIPLINARY RESEARCH

From self-assembly to quantum guiding: A review of magnetic atomic structures on noble metal surfaces

To cite this article: Cao Rong-Xing *et al* 2014 *Chinese Phys. B* **23** 038102

TOPICAL REVIEW — Magnetism, magnetic materials, and interdisciplinary research

From self-assembly to quantum guiding: A review of magnetic atomic structures on noble metal surfaces*

Cao Rong-Xing(曹荣幸), Zhang Xiao-Pu(张孝谱), Miao Bing-Feng(缪冰锋), Sun Liang(孙 亮), Wu Di(吴 镝), You Biao(游 彪), and Ding Hai-Feng(丁海峰)†

National Laboratory of Solid State Microstructures and Department of Physics, Nanjing University, Nanjing 210093, *China*

(Received 4 December 2013; published online 24 January 2014)

Recent advances in the study of magnetic atomic structures on noble metal surfaces are reviewed. These include one-dimensional strings, two-dimensional hexagonal superlattices, and novel structures stabilized by quantum guiding. The combined techniques of low-temperature scanning tunneling microscopy, kinetic Monte Carlo simulations, and *ab initio* calculations reveal that surface-state-mediated adatom-step and adatom–adatom interactions are the driving forces for self-assembly of these structures. The formation conditions are further discussed by comparing various experimental systems and the kinetic Monte Carlo simulations. Using scanning tunneling spectroscopy and tight-binding calculations together, we reveal that the spectra of these well-ordered structures have characteristic peaks induced by electronic scattering processes of the atoms within the local environment. Moreover, it is demonstrated that quantum confinement by means of nano-size corrals has significant influence on adatom diffusion and self-assembly, leading to a quantum-guided self-assembly.

Keywords: surface states, long-range interaction, self-assembly, quantum confinement

PACS: 81.07.–b, 73.21.–b, 68.37.Ef, 81.16.Dn **DOI:** 10.1088/1674-1056/23/3/038102

1. Introduction

Ordered arrays of magnetic nanostructures have attracted both theoretical and experimental interest due to their rich physical properties and potential applications.[1–15] Recent developments in nanoscience make it possible to fabricate structures and investigate their unique properties down to the atomic level. To date, two main approaches have been used: atomic manipulation through scanning tunneling microscopy (STM)[16–30] and self-assembly growth.[2,3,9,10,31–40] Atomic manipulation is an advantage in building structures in arbitrary geometry, while self-assembly can provide large-scale well-ordered structures spontaneously and more economically.

Self-assembly through substrate-mediated long-range interactions (LRI) between adatoms is a typical example.[8–10,41] LRI was first predicted 55 years ago by Koutecký[42] and was revealed to oscillate with a periodicity of half the Fermi wavelength and to decay with an increase in interatomic distance (by Grimley, Einstein, and Lau *et al.*)[43–45] Utilizing field ion microscopy, Tsong was the first to observe this effect on Re/W(110) system experimentally.[46,47] In 2000, Hyldgaard and Persson investigated the LRI on the noble metal surface through Shockley surface states.[48] When the surface has a free-electron-like surface-state band, the LRI decays more slowly, and the wavelength at the Fermi level is generally longer for surface states than for bulk states. Therefore, observing the LRI experimentally is expected to be easier in the presence of such a surface-state band and was indeed realized on Ag(111) and Cu(111) by low-temperature STM.[8,9,41,49] On Cu/Cu(111) and Co/Cu(111), locally ordered structures with six-fold symmetry were observed, while no superlattice was found. On Co/Ag(111), only a disorder-like distribution with a broad peak at preferred separation but without six-fold symmetry was reported. Interestingly, Ce/Ag(111) and Ce/Cu(111) at optimal conditions showed a well-ordered hexagonal superlattice up to a few hundred nanometers, regardless of the large in-plane lattice mismatches.[9,49] This is due to the fact that surface-state-mediated LRI is dominant at this diluted region and was revealed to be the driving force for superlattice formation, as also supported by kinetic Monte Carlo (KMC) simulations for Ce/Ag(111) and Fe/Cu(111).[50,51] They found that the following parameters play important roles in the superlattice formation: the repulsive ring, the distance and depth of the first minimum interaction, the diffusion barrier, and the concentration of deposited adatoms.

Except for the two-dimensional (2D) atomic superlattice mentioned above, one-dimensional (1D) atomic structures are also of enormous interest.[3,20,21,23–26,28,30,52,53] They are believed to have strong potential in future nanoscale electronic and magnetic devices. General features of electronic structure, magnetic properties, and interactions in 1D nanostructures on metal surfaces were revealed by previous theoretical studies.[11–15] A prototype device of

*Project supported by the National Basic Research Program of China (Grant No. 2010CB923401) and the National Natural Science Foundation of China (Grant Nos. 10974087, 11374145, 11304150, and 11023002).

†Corresponding author. E-mail: hfding@nju.edu.cn

nonvolatile information storage has been demonstrated in atomic chains, based on the magnetic coupling.[3,30] Moreover, recent studies suggest that 1D spin chains could be used for quantum communications.[28,53–56] In particular, magnetic atomic strings with a fixed interatomic distance were predicted to have both high speed and high fidelity in quantum information transfer.[55,56] A prototype device was recently demonstrated experimentally through the spin strings.[28,53] These 1D nanostructures were formed by atomic manipulation,[20,21,23–26,28,30] self-assembly on reconstructed surfaces,[53] and step decoration of vicinal surfaces.[3,52] In addition, surface-state-mediated adatom-step and adatom–adatom interactions[57,58] also give a new possibility for 1D atomic string formation near the step edges of noble metal (111) surfaces. Moreover, the exploration of their electronic properties is critical for mastering their functionalities.

Furthermore, atomic self-assembly was predicted to be influenced by a 2D quantum size effect (QSE) as the system size is reduced.[59] The QSE has been demonstrated to influence various properties such as atom diffusion,[60,61] growth stability,[62–68] optics,[69] magnetism,[70–72] transport,[73] and superconductivity.[74] The QSE in films is mainly focused on confinement in one dimension, the vertical direction, while more novel phenomena are expected to appear when electrons are confined in two dimensions. Pioneering work has already shown that spin-averaged and spin-polarized local density of states (LDOS) can be influenced by 2D quantum confinement.[17,75–78] It would be interesting to explore more properties under 2D quantum confinement, such as atom diffusion and self-assembly growth.

In this paper, we will review recent experimental and theoretical progress in the study of self-assembly of magnetic adatoms on noble metal surfaces, including 2D superlattices, 1D atomic strings, and structures stabilized by quantum-guided self-assembly. The formation mechanisms of these novel structures are discussed with the low-temperature STM exploration and KMC simulations. The electronic properties of these self-assembled structures are measured with low-temperature scanning tunneling spectroscopy (STS) and the underlying physics are explained with the tight-binding (TB) calculations. Moreover, it is demonstrated that quantum confinement by nano-size corrals has significant influences on the diffusion and self-assembly of adatoms, leading to quantum-guided self-assembly.

2. 2D self-assembly

2.1. Atomic superlattice

Self-assembly of magnetic adatoms on noble metal surfaces is typically studied in an ultrahigh vacuum chamber equipped with a low-temperature STM and in-situ evaporator. To avoid redundancy, we introduce only the experimental setup and procedure carried out by the low-dimensional magnetism group in Nanjing University. We believe the instruments and methods used in other groups are similar. The key techniques used for these studies are low-temperature STM and low-temperature deposition, typically at the STM stage. The in-situ sample cleaning and annealing apparatus are also necessary. Typically, the single-crystal Cu(111) and Ag(111) substrates are cleaned by repeated cycles of argon ion sputtering at 1.5 keV and annealing to 870 K. After that, the crystal is transferred into the STM stage and cooled to 4.7 K. The clean surfaces with low-impurity concentration are crosschecked by STM. The sample can be warmed up by a heater or be cooled down to 3.0 K by pumping liquid He in the cryostat. High-purity adatoms are deposited by means of electron-beam evaporation from a thoroughly outgassed rod onto the surfaces of substrates located at the STM stage at 6 K. The typical rate of deposition is 0.002–0.02 monolayer equivalent (MLE) per minute. Electrochemically etched and in-situ electron-beam cleaned tungsten tips are used for the STM measurements.[79] The bias voltage, U, refers to the sample voltage with respect to the tip.

A long-range-ordered hexagonal atomic superlattice was first observed experimentally in ~ 0.01 MLE Ce adatoms deposited on a Ag(111) surface (Fig. 1(a)).[9,10] The Fourier transform of this image (inset of Fig. 1(b)) confirms the well-ordered 2D hexagonal superlattice structure. The 3.2 nm periodicity of the superlattice is revealed by the histogram of the nearest-neighbor adatom–adatom separations shown in Fig. 1(b). The self-assembly of Ce adatoms on Ag(111) as a function of adatom concentration and of temperature were also investigated. When the adatom concentration is increased to 2%, a hexagonal superlattice is maintained at reduced interatomic distances of 2.2 nm, with more disorder induced by the increased concentration of Ce dimers. At even higher adatom concentration, more and more Ce dimers are found and the superlattice collapses into compact islands. Heating the sample up to 10 K causes the disappearance of the hexagonal superlattice. The formation and stability of the 2D hexagonal Ce adatom superlattice can be understood within the theoretical model of the interaction energy mediated by a Shockley surface-state band between two adatoms.[48] The authors concluded that the large-scale formation of the superlattice is governed by a subtle balance between the sample temperature, the diffusion barrier, and the concentration-dependent adatom interaction potential. On the other hand, many other systems that cannot form superlattices have been considered. On Cu/Cu(111) and Co/Cu(111), only locally ordered structures with six-fold symmetry were observed, while no superlattice was found.[8,41] On Co/Ag(111), a disorder-like distribution with a broad peak at the preferred separation but no six-fold symmetry was reported.[8] Therefore, uncovering the

presently unclear mechanism of superlattice formation is very important. To do this, the preparation process was separated into two processes (unlike the typical deposition at optimal growth temperature): the low-temperature growth and the following diffusion at higher temperature. This could give further insight for the mechanism of the 2D superlattice formation.

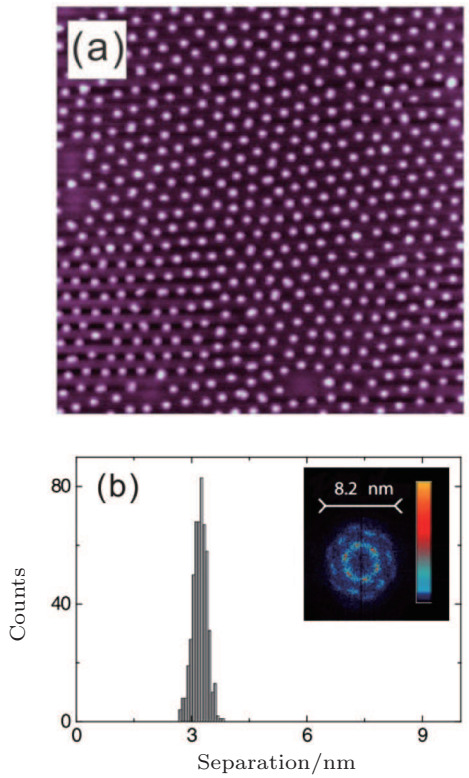

Fig. 1. (a) STM image of Ce superlattice on Ag(111) surface at 3.9 K (nominal coverage is ∼0.01 MLE, image size: 69×69 nm^2, $U = -0.1$ V, and $I_t = 10$ pA). (b) Histogram of the nearest-neighbor adatom–adatom separations in (a). Inset: the Fourier transform of the STM image (a).[10]

The growth of 2×10^{-3} MLE Fe adatoms on Cu(111) at 6 K is investigated and the typical STM image at 4.7 K is shown in Fig. 2(a).[80] We find that the Fe adatoms are immobile at 4.7 K, which suggests that the thermal energy is well below the diffusion barrier E_d. To obtain the statistics of the interatomic distance, the histogram of the nearest-neighbor separation of Fe adatoms is plotted in Fig. 2(b). We found that it follows a random distribution, as was naturally believed for a long time but had never been demonstrated. The random distribution function $f_{ran}(r)$ can be formulated through the concept that a given area statistically should have a constant concentration of adatoms. The formula with the correction for a square (typical shape for STM images) was first given by Knorr *et al.*[8] To characterize the diffusion barrier, the atomic-diffusion process of single Fe atoms on Cu(111) is investigated. To do this, about 5×10^{-4} MLE Fe atoms are deposited and the adatoms are well separated from each other (Fig. 3(a)). The scanning conditions are the sample bias $U = 0.1$ V and the tunneling current $I_t = 40$ pA. Under this condition, there is no apparent tip-induced atom-hopping at 4.6 K. Then the temperature is slowly raised to allow adatom hopping within a period of several minutes to several tens of minutes. We take consecutive scans with the rate of 78 s per frame to trace single-atom trajectories. The hopping rates at different temperatures are recorded and used to fit with the Arrhenius law: $\upsilon = \upsilon_0 \exp(-E_d/k_B T)$, where k_B is the Boltzmann constant and T is the temperature of the substrate. The fitting yields the diffusion barrier $E_d = 23.8 \pm 1.5$ meV and the attempt frequency $\upsilon_0 = 4 \times 10^{8\pm1}$ Hz (Fig. 3(b)). The measured diffusion barrier and the attempt frequency also explain why no apparent atomic diffusion is observed at 4.6 K.

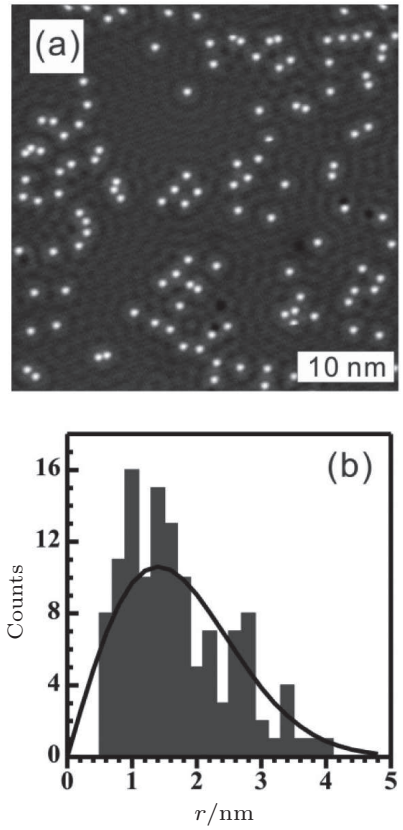

Fig. 2. (a) STM image of $\sim 2 \times 10^{-3}$ MLE Fe adatoms on Cu(111) at 6 K (image size: 40×40 nm^2, $U = 0.1$ V, and $I_t = 0.1$ nA). (b) Histogram (bar) of the nearest-neighbor distance obtained from many images as (a) and the calculated random distribution of the same coverage (line).[80]

As revealed by KMC simulations, surface-state-mediated LRI plays an important role in self-assembly formation.[50,51] To explore the LRI among the Fe atoms, we investigate the annealing effect for samples with different coverage. The annealing temperature is limited to < 12 K because of the noticeable increase in the number of dimers and clusters at higher temperatures. Figure 3(c) is a typical STM image of 4.2×10^{-3} MLE Fe on Cu(111) at 4.7 K, after annealing at 12 K for 5 min. The Fe atoms tend to stay away from each other at a preferred distance, even with some locally ordered structures. Through recording several images like Fig. 3(c),

the statistical histogram $f(r)$ of the nearest-neighbor Fe separation is obtained. The result is shown in Fig. 3(d) as columns where three peaks with decreasing amplitude are found. The highest peak appears at ~ 1.2 nm and the other two peaks are around 2.7 nm and 4.2 nm. As presented, the histogram oscillates with a period of 1.5 nm, which corresponds to half the wavelength at the Fermi level of the Shockley surface state on Cu(111). The observed histogram is clearly different from the random distribution function $f_{\rm ran}(r)$ at the same coverage (solid line in Fig. 3(d)), which evidences the existence of LRI among the Fe atoms. As established by Repp *et al.*[41] and Knorr *et al.*,[8] the LRI energy can be calculated according to Boltzmann's statistics: $E(r) = -k_{\rm B}T \ln[f(r)/f_{\rm ran}(r)]$. Therefore, the experimentally determined Fe–Fe LRI as a function of the adatom separation is shown in Fig. 3(e). The LRI oscillates with decreasing amplitude and a period of about 1.5 nm. The first minimum appears at about 1.1 nm with the depth of ~ 1.7 meV which agrees well with the previous experimental results[81] and the theoretical calculation by Stepanyuk *et al.*[82]

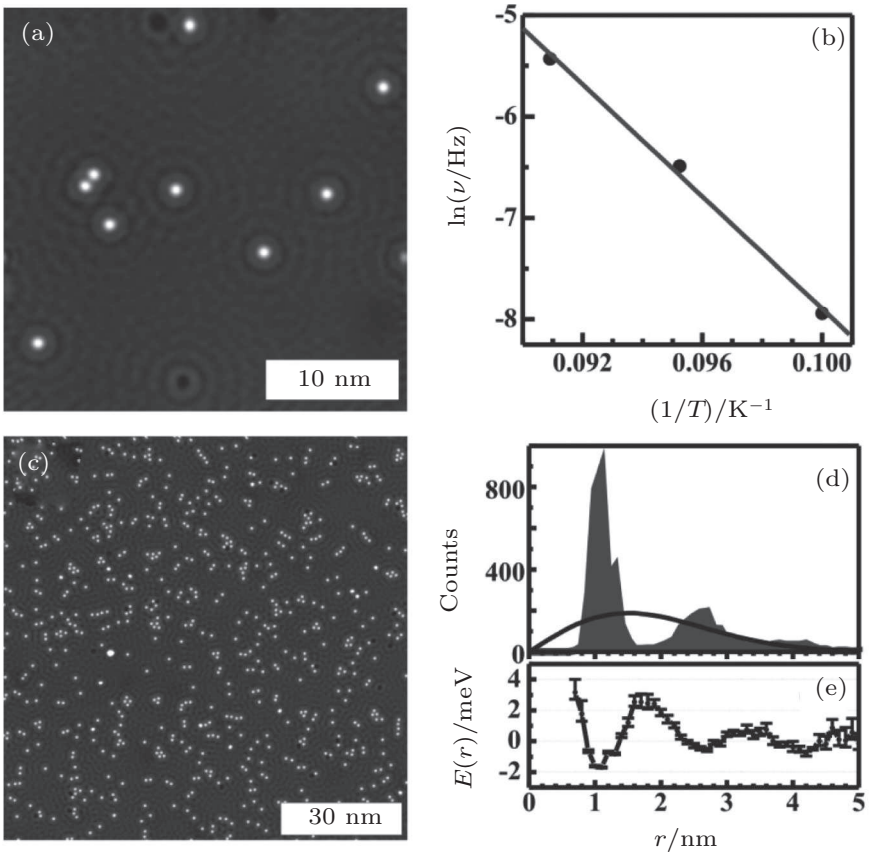

Fig. 3. (a) STM image of $\sim 5 \times 10^{-4}$ MLE Fe adatoms on Cu (111) (image size: 30×30 nm^2, $U = 0.1$ V, and $I_{\rm t} = 40$ pA). A sequence of images (78 s per frame) at different temperatures is used to derive the Arrhenius plot of the hopping rate of isolated Fe monomers (b).[80] (c) STM image of 4.2×10^{-3} MLE Fe monomers on Cu(111) obtained after annealing at 12 K for 5 minutes (image size: 100×100 nm^2, $U = 0.1$ V, and $I_{\rm t} = 0.1$ nA). (d) Histogram (bar) from seven images as (c) and the calculated random distribution of the nearest-neighbor distance (line). (e) The long-range interaction energy is derived from (d).[80]

With the experimentally determined position of the first minimum in the LRI energy, we can calculate the optimum coverage for the superlattice to be 4.5×10^{-2} MLE. The typical STM image for this coverage is presented in Fig. 4(a). We find the Fe atoms form an almost well-ordered hexagonal superlattice, with the exceptions appearing as some brighter spots: Fe dimers or clusters formed during deposition that have much higher diffusion barriers than a single Fe atom. To obtain the statistical information, we plot in Fig. 4(b) a histogram of the nearest-neighbor Fe separation derived from the STM image shown in Fig. 4(a). It shows a sharp peak around 1.2 nm with the half width of about 0.3 nm. For comparison, the random distribution function with the same coverage is plotted as the solid line in Fig. 4(b). The peak appears at a different position, and it is much broader than the experimental histogram. These results demonstrate that the 2D atomic self-assembly can occur for Fe adatoms on Cu(111).

We also try to form a superlattice of Fe on a different substrate, Ag(111). However, no matter how we tune the concentration and the annealing temperature, no well-ordered superlattice is observed. Comparing Fe on Cu(111) and Ag(111), we find that they have different diffusion barriers, even though

the LRIs are similar.[80] Negulyaev *et al*. pointed out that the formation condition is determined by the subtle balance between the LRI energy and the diffusion barrier.[50] Therefore, we compare the ratio between these two energies for different systems[8,9,41,49] and find that a well-ordered or quasi-ordered superlattice can be formed when the ratio is above 5%, as in Ce/Ag(111) and Fe/Cu(111). Otherwise, only locally ordered structures without long-range order or disorder-like structures are formed. The physical picture can be understood as follows. The atoms are randomly distributed during deposition and they need to undergo enough hopping to reach the ideal positions with small thermal broadening in order to form an ordered superlattice. The effect of the thermal broadening is determined by the ratio of the depth of the potential well versus the temperature. This ratio is proportional to the interaction energy versus the diffusion barrier since the temperature is governed by the diffusion barrier. The higher the ratio is, the less the thermal broadening and the better the superlattice. Therefore, the ratio is one of the critical parameters that determine the formation condition for the superlattice.

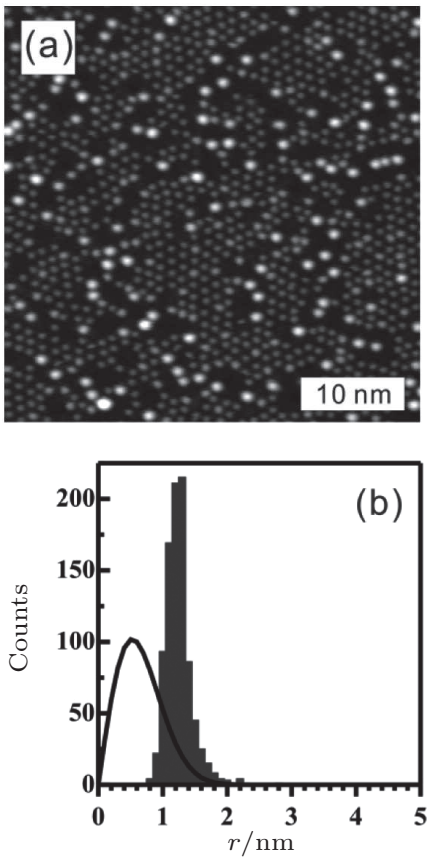

Fig. 4. (a) STM image of Fe quasi-superlattice on Cu(111) after annealing at 12 K (image size: 40×40 nm^2; coverage = 4.5×10^{-2} MLE, $U = 0.2$ V, and $I_t = 0.5$ nA). (b) Histogram (bar) from (a) and the calculated random distribution function of the given coverage (line).[80]

It was pointed out that the formation of the dimers and clusters can also dramatically influence the formation of the superlattice.[51] Dimers/clusters have much higher diffusion barriers than a single adatom. Therefore, they are anchored once formed, and they are unlikely to form at the ideal positions, and this will distort the well-ordered superlattice. This is verified in the experimental results of Ce/Ag(111) and Fe/Cu(111). For Ce/Ag(111), an almost perfect superlattice can be achieved,[9] while for Fe/Cu(111) with higher cluster concentration, only a quasi-superlattice is obtained. Therefore, low dimer/cluster concentration is important for superlattice formation. In addition, this concentration during the deposition process for the optimum coverage for forming the superlattice is proportional to a^2/b^2, where a is the repulsive ring radius referred to the position where the LRI has absolute maximum energy and b is the position of the first LRI minimum.[80] The upper limit of the specific value for a good-quality superlattice formation is about 19% through summarization from several experimental systems.[9,80] Besides the dimer formation during the deposition process, the dimer can also be induced when the thermal energy approaches the energy maximum during the annealing process. This is because the adatoms can cross the repulsive energy barrier at a and form dimers with the assistance of the thermal energy.

To further verify the proposed mechanism, KMC simulations are carried out. In the simulations, the hopping rate of an adatom from site i to site j on the (111) surface is calculated using the Arrhenius law $\upsilon_{i\to j} = \upsilon_0 \exp(-E_{i\to j}/k_{\rm B}T)$, where $E_{i\to j}$ is the hopping barrier. The influence of the LRI through the surface-state electrons is included in the hopping barrier, i.e., $E_{i\to j} = E_{\rm d} + 0.5(E_j - E_i)$,[83,84] where E_i (E_j) is the total energy caused by the LRI. We first limit the dimer formation in the simulations, and the effect of dimer formation will be discussed later. In order to show the effect of $E_i/E_{\rm d}$, the diffusion barrier is also artificially varied while the interaction energy is kept the same as that of Fe/Cu(111). The simulated results of 4.5×10^{-2} MLE adatoms at 4 K for three different diffusion barriers are shown in Figs. 5(a)–5(c). In order to obtain sufficiently high adatom hopping rates, we choose different annealing temperatures according to the respective diffusion barriers. With the ratio corresponding to Fe/Cu(111), the simulation yields an excellent superlattice and the Fourier transform of the image shows a sharp hexagonal pattern in Fig. 5(a). When $E_{\rm d}$ increases to 37.5 meV, some adatoms start to deviate from the ideal positions and the Fourier transform still shows a hexagonal pattern, but the spots are a little bit blurred in Fig. 5(b). When $E_{\rm d}$ further increases to 50 meV, the hexagonal pattern disappears and the Fourier transform only shows rings, indicating that the disorder is dominant. These simulation results demonstrate that $E_i/E_{\rm d}$ higher than 5% is required to obtain a good-quality superlattice in the absence of dimer formation. When $E_{\rm d}$ is 25 meV and the dimer/cluster formation is included, the superlattice in Fig. 5(a) is strongly influenced

(Fig. 5(d)). One can also find locally hexagonal structures in the region with a low concentration of dimers. This agrees well with the experimental findings for Fe/Cu(111) (Fig. 4(a)). The slight deviation may come from choosing to omit the dimer hopping from the simulations: the dimer hopping barrier is estimated to be about twice the diffusion barrier of a single adatom.[85] When hopping is included, a better agreement is expected. In addition, the dimer appears as a single object in the experimental images while it was plotted as two atoms in the simulation result, which may create different visual impressions.

Above, we discuss the formation mechanism for the 2D superlattice, and the formation conditions for a good superlattice is found. It would be interesting to further apply this to explore new potential systems. So far, the experimentally-found good systems are Ce/Ag(111) and Fe/Cu(111). Fe is a 3d element while Ce is a lanthanide. It would be easier to find a system similar to Ce/Ag(111) since lanthanides have identical outer shell electron configurations. As the LRI is intrinsically a Coulomb interaction, it should be mainly determined by the outer shell electrons. Therefore, it would be expected that lanthanides have similar LRIs on a given surface such as Ag(111). It is also expected that they have almost the same interactions with the Ag substrate. The atomic radii of lanthanides are also similar, varying only from 0.173 to 0.204 nm. Thus, they may have similar diffusion barriers on Ag(111). We picked Gd as our test system, as it has a large magnetic moment with potential applications in magnetic devices. Figure 6(a) shows the typical image for 8.0×10^{-3} MLE Gd on Ag(111), obtained at 3.5 K. The scanning conditions are $U = -100$ mV and $I_t = 2$ pA. Interestingly, Gd atoms form a well-ordered hexagonal superlattice with a period of 3.0 nm on Ag(111), as speculated. The Fourier transform also shows a good hexagonal pattern (inset of Fig. 6(a)), with a visible second-order diffraction pattern. Then, the measurements of the diffusion barrier and LRI are performed, similar to those for Fe/Cu(111). The diffusion barrier of Gd atoms on Ag(111) is about 7.6 meV,[86] which is similar to 10 meV of Ce/Ag(111).[9,10] The LRI has the depth of the first minimum about 0.6 meV and oscillation period of 3.8 nm, which is also similar to Ce/Ag(111).[9,10,86] The speculation of self-assembly for lanthanides on Ag(111) is verified in two systems, and this could be further extrapolated to the whole group of lanthanides.

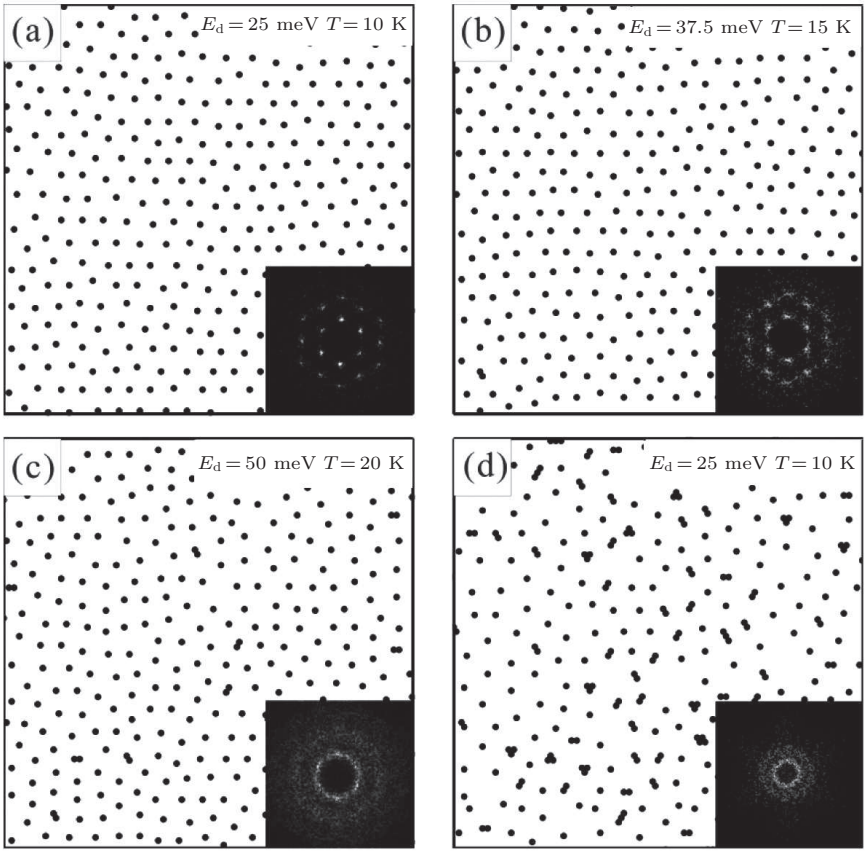

Fig. 5. KMC simulated results of adatoms on the Cu(111) surface with various diffusion barriers. All the image sizes are 20×20 nm^2. The same experimental determined Fe–Fe LRI energy is used for all images. (a)–(c) exclude the dimer formation in the simulation and use 25, 37.5, and 50 meV as the diffusion barrier, respectively. (d) uses 25 meV as the diffusion barrier but includes the dimer formation. Insets: Fourier transform of each image.[80]

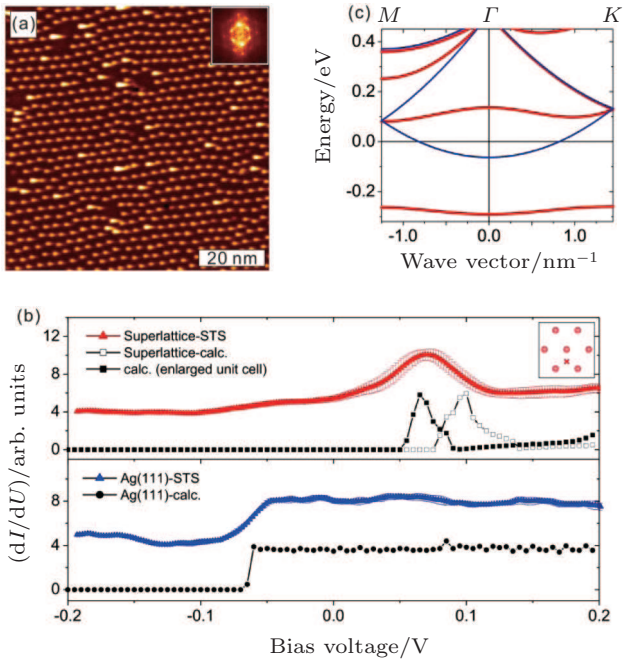

Fig. 6. (a) STM image of Gd superlattice on Ag(111) at 3.5 K (coverage = 8.0×10^{-3} MLE, $U = -100$ mV, and $I_t = 2$ pA). Inset: Fourier transform of the image.[86] (b) The experimental dI/dU spectra (red triangles) and the tight-binding calculated LDOS (open black rectangles: 10×10 unit cell, solid black rectangles: 11×11 unit cell) of the superlattice are shown in the upper panel. The dI/dU spectra are measured at the position indicated by the cross in the inset. Lower panel shows the experimental (blue triangles) and calculated (black circles) spectra of the bare Ag(111) surface. The experimental results have been shifted vertically for clarity. (c) Calculated band structures of the superlattice (red line) and the bare Ag(111) surface (blue line).

2.2. Spectroscopic study of 2D superlattices

The electronic properties of these self-assembled structures are critical for their functionalities. STS provides the best tool to investigate these electronic properties since it can be readily applied after the morphology measurements. The first study was performed on the Ce superlattice on the Ag(111) system.[87] In the following, we will present the study of a similar system, the Gd superlattice on Ag(111), as mentioned above. After obtaining the topographic information of the created structures, we perform STS measurements to reveal the characteristic electronic properties of these self-assembled structures. As a reference, we first take dI/dU spectra on the clean and wide Ag(111) terrace to check the tip's condition. The scanning conditions are $U = 150$ mV and $I_t = 0.5$ nA. The surface-state band that starts at about 67 meV below E_F is clearly observed (blue triangles in the lower panel of Fig. 6(b)), which is in good agreement with previous findings.[88] Due to the tip-induced adatom motion, the dI/dU spectra on the top of the Gd adatoms are not very well reproducible. Therefore, we focus our study on the dI/dU spectra obtained at the center of the triangle formed by three Gd adatoms in the superlattice, shown as the red triangles in the upper panel of Fig. 6(b) (location of taking spectra is indicated as the cross in the inset). Furthermore, we find that the LDOS shows a peak at ~70 meV above E_F, which is similar to the peak found in Ce/Ag(111).[87]

To understand the experimental results, TB calculations similar to previous study in Ce/Ag(111)[87] are performed. The TB Hamiltonian is described as $H = t \sum_{\text{n.n.}} |i\rangle\langle j| + \sum_i (\varepsilon_0 + V_i)|i\rangle\langle i|$, where t is the isotropic hopping integral, ε_0 is the on-site potential of the bare Ag(111) lattice, and V_i describes the correction to the on-site potential induced by adatoms. The values of $t = -0.75$ eV and $\varepsilon_0 = 4.437$ eV are taken to best reproduce the experimentally determined onset energy and the effective mass of Ag(111) surface states.[88] The local V_i is set to be V_{nn} at the three nearest-neighbor Ag atoms supporting the adatom, and 0 elsewhere in each unit cell. We use a 44×44 unit cell to adjust V_{nn} to reproduce Friedel oscillations near the adatom. With this, we find V_{nn} to be -1.7 ± 0.2 eV. The obtained parameters are used to calculate the electronic states of the self-assembled structures with the TB approximation.

The calculated energy band of Ag(111) is shown in Fig. 6(c) as blue lines and the LDOS is further obtained in the lower panel of Fig. 6(b) as black circles. The calculated spectra show that the typical surface state of Ag(111) is a step function at 67 meV below E_F, which agrees well with the experimental findings.[88] Then, we further calculate the electronic states of the superlattice, choosing a unit cell of 10×10 to present the periodicity of the Gd superlattice. After periodic arrangement of Gd adatoms, the gap opening near E_F occurs (red lines in Fig. 6(c)). From the results calculated at the center of the triangle formed by three Gd adatoms in the superlattice, one can see that LDOS has a feature similar to the experiments and shows a peak around 100 meV (open black rectangles in the upper panel of Fig. 6(b)). The experimental results have been shifted vertically for clarity. This theoretical peak position is slightly higher in energy than the experimental value. We attribute this difference to the effect of tip-induced separation increasing between the Gd adatoms in the superlattice. As discussed by Ternes *et al*., the peak shifts to lower energy when the separation between atoms increases.[87] In our measurements, we have to use a higher tunneling current, $I_t = 0.5$ nA (the typical value used for obtaining the topography is 2 pA), to perform dI/dU spectra measurements in order to achieve a satisfying signal-to-noise ratio. The measurements are performed with the click mode. Occasionally, we find a local distortion of the superlattice after performing the STS measurements. Typically, the tip will enlarge the separation between the Gd adatoms, therefore, we also made the calculations with a slightly larger unit cell, 11×11. The obtained LDOS has a similar shape except that the peak shifts down to about 65 meV (solid black rectangles in the upper panel of Fig. 6(b)). Therefore, we believe the slight difference between the experimental and calculated results comes from tip-induced distortion.

3. 1D self-assembly

3.1. Atomic strings

Dimensionality is one of the typical criteria to group materials and it can have a strong influence on a material's properties. Above, we discussed the investigation of a 2D superlattice of magnetic atoms. It would be interesting to explore further whether it is possible to self-assemble the 1D atomic structure. 1D atomic structures are believed to have great potential in future nanoscale electronic and magnetic devices. A prototype device for nonvolatile information storage has been demonstrated in atomic chains, based on magnetic coupling.[3,30] Moreover, recent studies suggest that 1D spin chains could be used for quantum communications.[28,53–56] Especially, the magnetic atomic strings with a fixed interatomic distance, were predicted to have both high speed and high fidelity in quantum information transfer.[55,56] The prototype device was recently demonstrated experimentally in spin strings assembled by atomic manipulation.[28,53] As discussed in the 2D self-assembly, the adatoms in the superlattice have a fixed separation between each other. In the following, we will show it is also possible to fabricate the 1D magnetic atomic strings in combination with the LRI and step-guiding.

Figure 7(a) presents a typical topographic image of 8×10^{-3} MLE Fe atoms on a vicinal Cu(111) surface with the average terrace width of about 5 nm after annealing to 13 K. Well-ordered atomic strings with a fixed separation are indeed formed near the upper step edges. Only a few atoms/clusters still exist on the top of the terrace, which could be caused by the pinning effect of defects in the terrace or by insufficient space near the adatom-occupied step edge. Moreover, the quantitative information about atomic strings is obtained in a zoomed-in image (Fig. 7(b)). Fe adatoms are separated by a fixed distance of 1.2 ± 0.1 nm (A–A' in Fig. 7(c)) and they are typically 0.8 ± 0.1 nm away from the step edge (B–B' in Fig. 7(d)). Occasionally, a few adatoms also appear closer to the step edge (C–C' in Fig. 7(d)), which may be anchored there during the deposition process. These demonstrate that a 1D atomic structure can also be self-assembled.

To understand the mechanism, *ab initio* calculations are performed. The calculated interaction energy between an Fe adatom and the nearby step on Cu(111) is shown in Figs. 8(a) and 8(b).[89] The interactions for the lower and upper terraces are both oscillatory, with a period of about 1.5 nm (half of the Fermi wavelength of the surface state of Cu(111)). The calculated results show that the adatom moving toward a step is repelled by the repulsive potential. For the lower and upper terraces, the first repulsive barrier occurs at distances of about 0.4–0.5 nm from the step edge. The strength of the repulsive barrier on the upper terrace (173 meV) is much larger than that on the lower terrace (26 meV), which is related to a redistribution of the electron-charge density at the step edge.[90] The first minimum of the interaction energy appears at ~0.9 nm on the lower terrace and at ~0.8 nm on the upper terrace. However, the depth of this minimum on the upper terrace (8 meV) is twice as large as that on the lower terrace (4 meV). At 10–11 K, Fe adatoms can easily be trapped in these attractive potential wells after overcoming small repulsive barriers at larger distances. According to Boltzmann distribution $\exp(-E_1/k_BT)$ (where E_1 is the depth of the first minimum of the interaction energy), one can easily find that the occupation probability in the potential well near the edge of the upper terrace is about 100 times larger than that on the lower terrace at 10–13 K. Therefore, Fe adatoms will be located at about 0.8 nm from the step edge on the upper terrace.

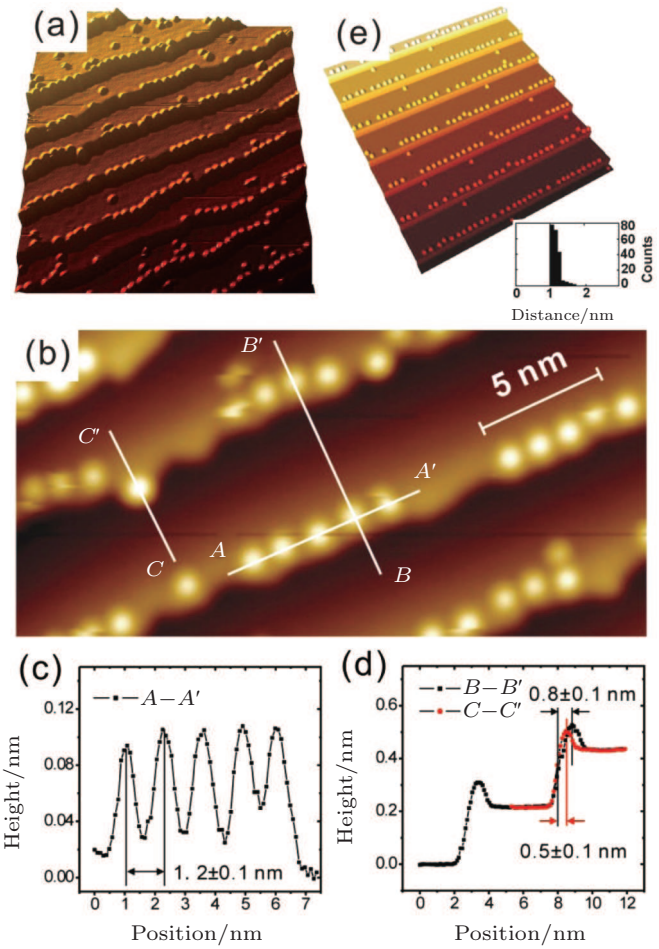

Fig. 7. (a) The STM image of Fe atomic strings on a vicinal Cu(111) surface (image size: 40×40 nm^2, coverage $=8\times10^{-3}$ MLE, $U=-0.8$ V and $I_t=1$ nA). (b) A zoomed-in image of (a). (c) and (d) Line profiles along and perpendicular to the string directions as marked in (b). (e) The kMC simulations of the self-organization of Fe adatoms on vicinal Cu(111) into atomic strings. The inset shows the statistics of the nearest-neighbor Fe–Fe separation along the step edges, which is centered in a narrow range around 1.2 nm.[89]

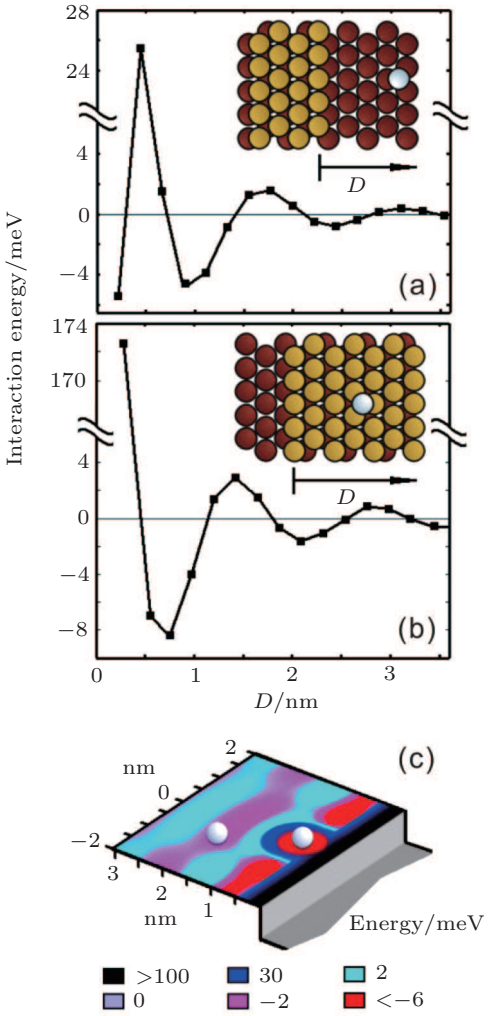

Fig. 8. Long-range interaction energy between the Fe adatom and the Cu step on Cu(111) (a) for the lower terrace and (b) for the upper terrace. (c) Potential-energy map for the Fe adatom to approach another Fe adatom trapped in the potential well near the edge of the upper terrace.[89]

If there are several Fe adatoms diffusing on the terrace of Cu(111), adatoms are captured near the step edge and they should interact with each other. Figure 8(c) presents the potential-energy map for the Fe adatom approaching another Fe adatom trapped in the potential well near the step edge of the upper terrace.[89] The repulsive area surrounding this adatom is easily seen and corresponds to the repulsive ring in the Fe–Fe LRI mentioned above. It is easier for the Fe adatom to approach the step edge within a distance of about 1.2 nm from the first Fe adatom, which is related to the first minimum of the Fe–Fe LRI. Fe adatoms interact with each other as well as the step edge and further form a sparse atomic string with an interatomic distance around 1.2 nm.

Following closely the experimental conditions, KMC simulations of the growth process of Fe adatoms on a stepped Cu(111) surface are carried out.[89] The surface-state-mediated adatom-step and adatom–adatom interactions are included in the simulations. The simulated results in Fig. 7(e) nicely demonstrate the self-organization of Fe adatoms into atomic strings at the edge of the upper terraces. The distribution of the interatomic distances along the string shows a pronounced peak around 1.2 nm (inset of Fig. 7(e)) and the string is 0.8 nm away from the step edge, in good agreement with the experimental findings. The simulated results unambiguously prove that the surface-state-mediated interactions between adatoms and steps are the driving force for the 1D self-assembly of atomic strings.

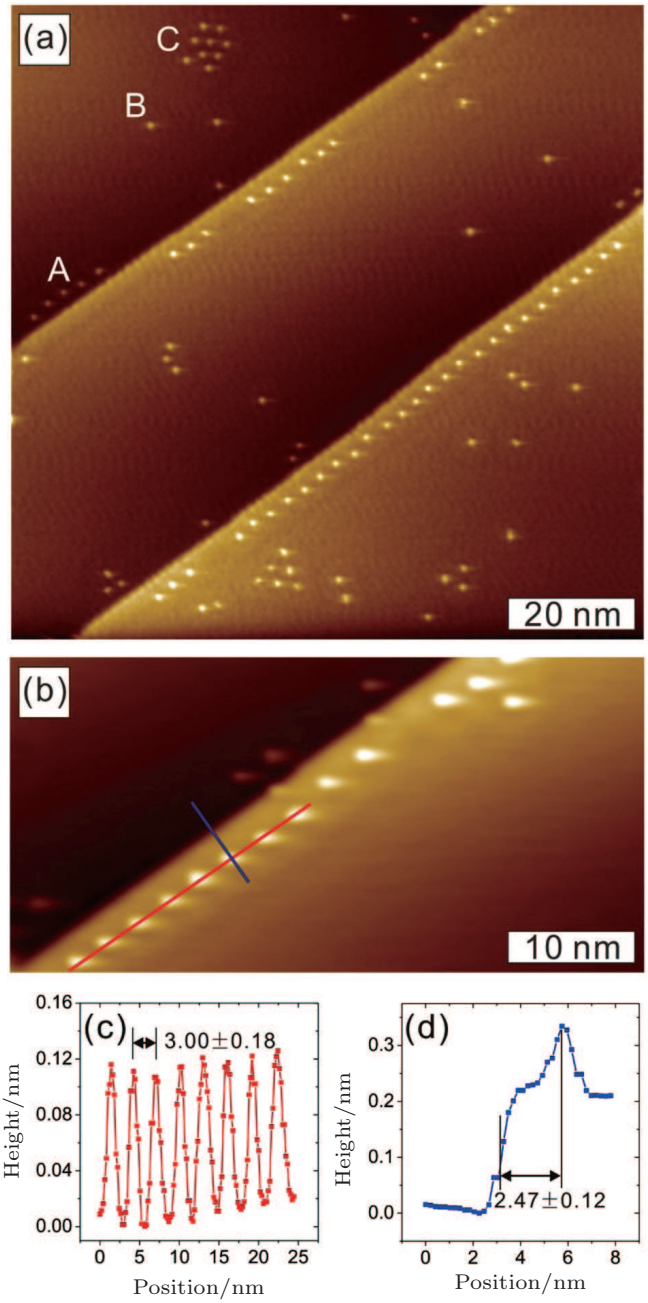

Fig. 9. (a) STM image of Gd atomic strings near the step edges of Ag(111) at 3.8 K (coverage = 1.0×10^{-3} MLE, $U = 100$ mV and $I_t = 2$ pA). (b) A zoomed-in image of the atomic string. (c) and (d) Line profiles along and perpendicular to the string direction as marked in (b), respectively.[91]

This 1D atomic string can also be formed in Gd/Ag(111) where 2D superlattice exists.[91] Figure 9(a) shows the typical image for 1.0×10^{-3} MLE Gd atoms on Ag(111) obtained

at 3.8 K. Well-ordered atomic Gd strings near the step edges on the upper terrace are observed. A few atoms also aggregate near the lower step edges (mark A), indicating that LRI between adatoms and steps exists at both the upper and lower terraces near the step edges. Moreover, a few single adatoms (mark B) and locally hexagonal structures (mark C) are found on the flat terrace. Due to a lower diffusion barrier compared to Fe/Cu(111), the single Gd adatom and hexagonal structures with similar size are typically mobile at this temperature on a flat terrace without defects. Therefore, we attribute these exceptions to the pinning effect induced by the substrate defects and subsequent aggregation near the pinned adatom driven by the Gd–Gd LRI. Through quantitative investigation of the zoomed-in image (Fig. 9(b)), the nearest-neighbor Gd separation of 3.0 ± 0.2 nm (Fig. 9(c)) and distance of 2.5 ± 0.1 nm to the step edge (Fig. 9(d)) are obtained. The Gd–Gd separation is consistent with the results of 2D hexagonal superlattice and the Gd–Gd LRI discussed previously.[86]

3.2. Spectroscopic study of 1D atomic string

After obtaining the topographic information of the atomic strings, low-temperature STS measurements are performed to reveal the characteristic electronic properties of this self-assembled structure.[91] The scanning conditions are $U = 150$ mV and $I_t = 0.5$ nA. As a reference, the spectra on the clean and wide Ag(111) terrace are first taken to check the tip's condition and the result is similar to the one shown in Fig. 6(b). The $\mathrm{d}I/\mathrm{d}U$ spectra are measured at the center of two neighboring adatoms in a string, shown as red triangles in the upper panel of Fig. 10(a) (location of taking spectra is indicated by the cross in the inset). The LDOS of the sparse string has a peak at approximately 65 meV above E_F. The unoccupied electronic states were also observed in previous STS results of close-packed one-dimensional chains.[20,23,25,26,52]

TB calculations are also performed similarly to those for the Gd superlattice on Ag(111).[91] The 10×250 unit cell is chosen to describe the isolated atomic strings, considering the interatomic separation of 3.0 nm (Model I in Fig. 10(b)). Gd and Ag atoms are indicated by red and gray spheres, respectively. Due to different on-site potentials, the three nearest-neighbor Ag atoms supporting the Gd adatom are indicated by dark blue spheres. The calculated LDOS based on Model I is plotted as black circles in the lower panel of Fig. 10(a) and it shows a curve with a step shape, in sharp contrast with the experimental finding.

Comparing Model I with the detailed experimental geometry of Gd atomic string, we realized that the step edge may play an important role. Therefore, we introduced the step edge to make the model closer to the actual environment of the strings (Model II in Fig. 10(c)). The upper and lower step edges are modeled as two Ag atomic rows whose on-site potentials are $V_{up} = +0.6$ eV and $V_{lw} = -0.6$ eV, respectively. These two potentials are determined to best reproduce the $\mathrm{d}I/\mathrm{d}U$ oscillation near the Ag(111) step edges experimentally determined by STS.[88] The calculated LDOS based on Model II shows a peak around 100 mV with a similar shape to the experiments (black rectangles in the upper panel of Fig. 10(a)). This agreement verifies the important contribution of the step edges to the spectroscopy of self-assembled atomic strings. The slight difference in peak position may come from the tip-induced lattice enlargement of Gd strings, similar to that in the Gd superlattices discussed above.

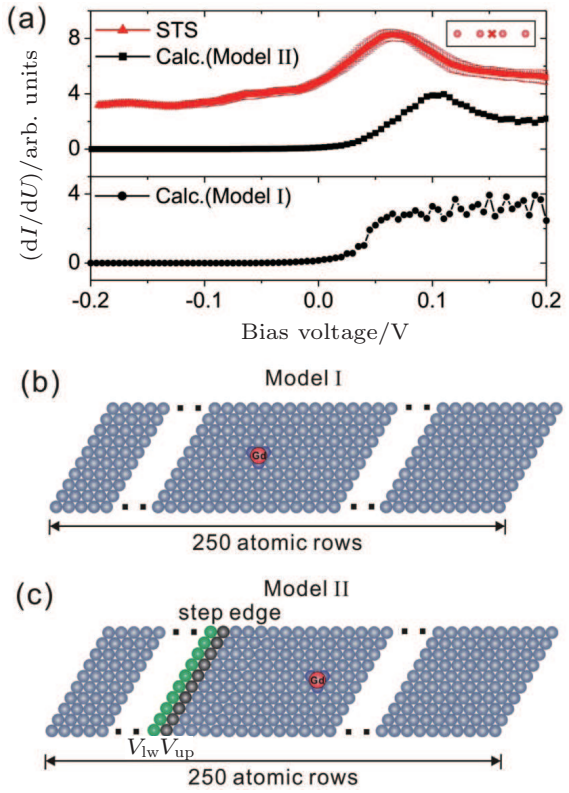

Fig. 10. (a) Upper panel shows the experimental $\mathrm{d}I/\mathrm{d}U$ spectra (red triangles) and the tight-binding calculated LDOS (black rectangles) using Model II of the Gd atomic string shown in (c). The $\mathrm{d}I/\mathrm{d}U$ spectra are measured at the position indicated by the cross in the inset. Lower panel shows the calculated spectra of the Gd atomic string using Model I shown in (b). The experimental results have been shifted vertically for clarity. In Model II, the upper and lower step edges are modeled as two Ag atomic rows whose on-site potentials are V_{up} (black spheres) and V_{lw} (green spheres), respectively.[91]

The importance of the step edge is further confirmed by the spectroscopic study of Fe strings on a flat terrace and near step edges constructed by atomic manipulation.[91] Fe adatoms have higher diffusion barrier on Ag(111) than Gd adatoms[80,86] and they are immobilized after positioning at 4.7 K. Figure 11(a) presents the isolated Fe atomic string on a flat terrace of Ag(111) with a period of 3.0 nm. The experimental $\mathrm{d}I/\mathrm{d}U$ spectra (red triangles), and TB calculated LDOS (black rectangles, based on Model I) of the isolated string are shown in Fig. 11(c). The experimental results indeed have a step shape and agree well with the theoretical re-

sults, except for the peak around −280 meV and the surface state of Ag(111) which is not suppressed. We attribute the exception to the simplicity of the effect of an adatom's potential on Ag electrons. The agreement in the isolated atomic string further confirms the importance of the detailed experimental geometry, i.e., the step edge near the self-assembled string.

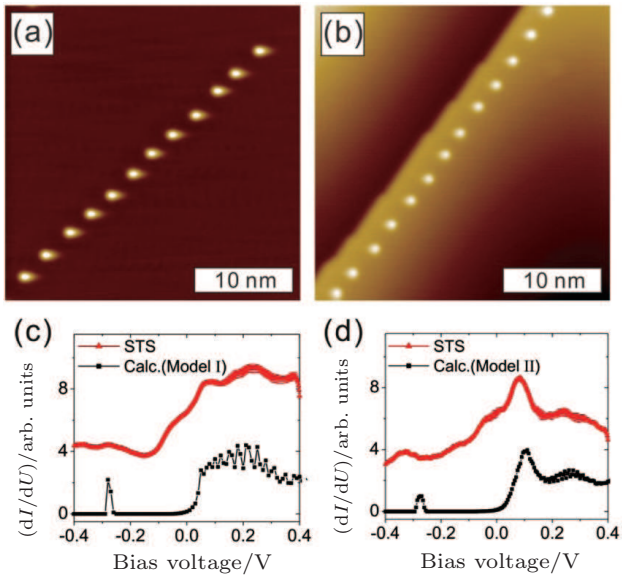

Fig. 11. STM images of the Fe atomic strings on a flat terrace (a) and near the step edges (b) of Ag(111) at 4.7 K built by atomic manipulation ($U = -1$ V and $I_t = 1$ nA). The experimental dI/dU spectra (red triangles) of strings in (a) and (b) and their tight-binding calculated LDOS (black rectangles) using the Model I and II in (b) and (c) of Fig. 10, are presented in (c) and (d), respectively. The dI/dU spectra are measured at the position indicated by the cross in the inset. The experimental results have been shifted vertically for clarity.[91]

Moreover, the Fe atomic string near the step edge of Ag(111) is also built by atomic manipulation (Fig. 11(b)). It has the same separation from step edges as the self-assembled Gd atomic strings. The experimental dI/dU spectra at the center of two neighboring adatoms in a Fe string (red triangles in Fig. 11(d)) have features similar to Gd strings and show a slightly larger peak around 85 meV. The calculated LDOS based on Model II shows a peak around 100 mV and agrees with the experiment, with the same exception as the isolated Fe string (black rectangles in Fig. 11(d)). The comparison of Fe strings on the flat terrace and near the step edges further evidences that the scattering of Ag(111) surface-state electrons by both the atoms of the strings and nearby step edges should be considered for the self-assembled string system guided by the step edges.

4. Self-assembly under 2D quantum confinement

As mentioned in the introduction, atomic manipulation is one of the important approaches for creating atomic structures in an atom-by-atom fashion. However, it also has the limitation that the speed is rather slow. Moreover, as size shrinks to the 10-nm range, quantum effects appear and can influence many system properties. For instance, when electrons are confined in the vertical direction, it has been found that quantum confinement has a decisive influence on the growth of thin films, resulting in novel effects.[62–67] If quantum confinement in the lateral direction could also be imposed, this would open the possibility for local functionality design with $<$ 10-nm resolution.

Recently, the quantum size effect was proposed to influence self-assembly and atomic diffusion.[59,61] Negulyaev *et al*. built a quantum resonator from two parallel monatomic Cu chains on Cu(111) at 12 K and studied the diffusion behavior of a single Cu adatom inside the resonator (Fig. 12(a)).[61] Surface-state electrons were confined in the resonator, forming clearly visible standing waves. In order to study the effect of quantum confinement on the atomic diffusion, KMC calculations were performed, and the calculated probability is presented in Fig. 12(b). There are three diffusion channels with a high probability to find the adatom, which is different from the 2D random walk of the adatom on the wide Cu(111) terrace.[61] Under the confinement, the adatom between the channels will first diffuse toward one of the channels and then migrate inside the channel parallel to the resonator walls. If more adatoms are introduced into the resonator, the interaction between them could result in the formation of a sparse string. Such structures have been recently observed inside self-assembled methionine nanogratings on Ag(111).[92] The quantum confinement on the atomic diffusion in the corral was also investigated.[59] The probability of finding a single Co adatom inside the pinned Co corral at 15 K was calculated by KMC simulations. The result shows several orbits of adatom motion with a high probability (Fig. 12(c)). When introducing more adatoms into a corral, they could occupy the diffusion orbits and form novel structures. Figure 12(d) shows the KMC calculated self-assembly of 0.01 MLE Ce adatoms inside the circular Ce corral made of Ce dimers on Ag(111) at 4 K. The Ce adatoms are self-organized into different concentric circular orbits, forming a "quantum onion".[59] These simulations demonstrate that quantum confinement can engineer the atomic diffusion and create novel atomic structures.

To further reveal the effect of quantum confinement, a circular quantum corral with 30-nm diameter is built with 32 Fe adatoms on Ag(111), as shown in Fig. 13(a). The slightly brighter spots are Fe dimers accidently formed during the manipulation. Surface-state electrons contained by Ag(111) are confined within the corral by strong scattering at the corral walls, leading to a concentric circular standing-wave pattern. This kind of pattern can be observed by the spectroscopy image as shown in Fig. 13(b). An average line profile from the center to the Fe circle, indicated by the black line, is plotted in the inset of Fig. 13(b). The average period of the stand-

ing wave is ∼ 3.8 nm, which corresponds to half of the Fermi wavelength of the Ag(111) surface state. About 0.02% MLE of Gd adatoms were deposited on the pre-patterned Ag(111) surface, and adatom diffusion on flat terraces and inside the corrals were studied. On a flat terrace without quantum corrals, we find the Gd adatoms follow a 2D random walk, similar to that observed for the diffusion of Cu single adatoms on a flat Cu(111) surface.[61] To obtain statistics on Gd adatom's diffusion inside the corral, we continued to image the same area until the liquid He in the cryostat evaporated. We collected hundreds of consecutive images and averaged them into a single image. With further background subtraction to remove the electronic effects caused by the corral, the statistical result was obtained.[93] For one adatom diffusing inside the corral, it is found that the adatoms stay mostly in the vicinity of a specific location and form an arc-shaped distribution near one side of the Fe corral, which is in contrast to theoretically predicted circular orbits.[59] This may be due to the fact that the Fe adatoms in the experiments are not positioned in as perfect a circle as in the theory, resulting in preferred occupation sites. To verify this, we repeated the measurements with new corrals and found that the arcs are always located near one side of the corral, but at different locations for different experiments. The random distribution of arcs suggests they are preferred occupation sites.

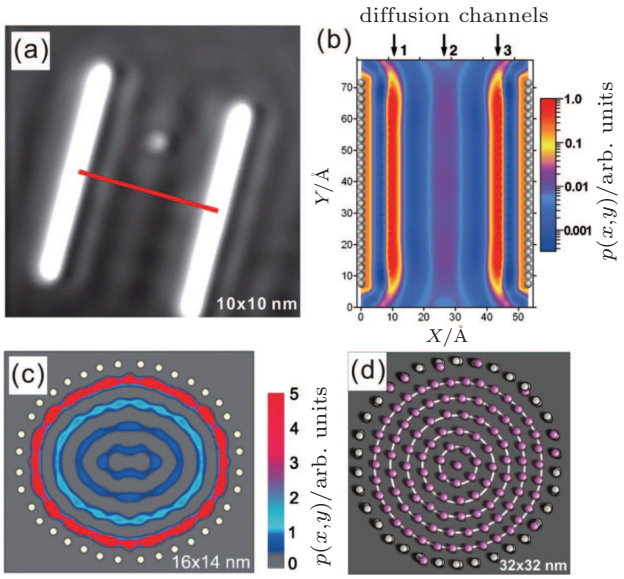

Fig. 12. (a) A single Cu adatom inside a quantum resonator built from two parallel monatomic Cu chains on Cu(111) at 12 K ($U = 0.1$ V and $I_t = 70$ pA). The distance between the chains is 5.5 nm. (b) The KMC calculated probability of finding the randomly walking Cu atom inside the resonator at 12 K.[61] (c) The calculated probability of finding a single Co adatom inside the pinned Co corral at 15 K. (d) "Quantum onion": self-assembly of 0.01 MLE Ce adatoms inside the circular Ce corral (radius: 15 nm) made of Ce dimers on Ag(111) at 4 K.[59]

To overcome the problem of Gd adatom trapping at preferred occupation sites, two Gd adatoms are introduced into the circular Fe corral by electron-beam evaporation (Fig. 13(c)). The idea was to use the collision of two adatoms to kick an adatom out of the preferred occupation site where it is trapped. To obtain statistics of the Gd diffusion inside the corral, more than 500 consecutive images are collected and the statistical result is shown in Fig. 13(d). The statistical result shows three concentric orbits of adatom motion and one focused at the center with separation of about 3.8 nm. The orbits have different intensities, suggesting that they have different occupancies. The brighter the orbit is, the higher the occupancy is. On the outermost orbit of Fig. 13(d), there are a few bright spots with much higher probability which correspond to the preferred occupation sites due to the imperfect circle. KMC simulations for the diffusion inside the corral considering the Fe–Gd and Gd–Gd LRI agree well with the experimental findings. The similarity between the distribution of the adatom diffusion probability and the LDOS demonstrates that the quantum confinement can significantly modify the atomic diffusion.

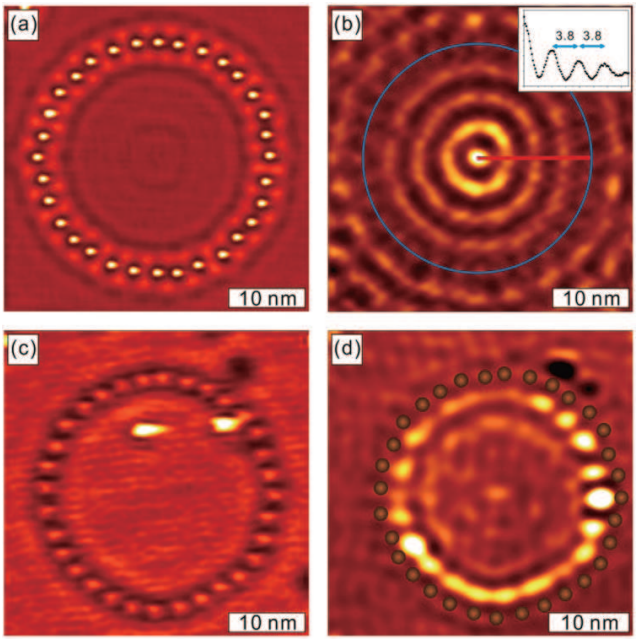

Fig. 13. (a) STM topography of circular corral built with 32 Fe adatoms on Ag(111) ($U = 100$ mV and $I_t = 1$ nA). (b) LDOS near E_F inside the corral. Fe circular corral is indicated by blue circle for clarity. Inset: average period of standing wave indicated by black line in (b) is ∼ 3.8 nm which corresponds to half of the Fermi wavelength of Ag(111). (c) Typical STM image of two Gd adatoms inside a circular corral. (d) Adatom probability distribution derived from summing up 510 successive images as in (c). For clarity, small balls are used to mark the positions of Fe adatoms.[93]

Moreover, the size-dependent quantum diffusion of Gd adatoms within Fe nano-corrals on Ag(111) are also carried out.[94] Figure 14(a) shows the spatial distribution of the LDOS near E_F within the circular Fe quantum corrals with the diameters of 6, 10, and 14 nm. The scanning condition for LDOS maps is $U = 20$ mV and $I_t = 1$ nA. To guide the readers, small balls were used to mark the position of Fe atoms. Inside the quantum corrals, an interesting periodic evolution

of LDOS is found as the diameter increases. One spot with high LDOS located at the center of the corral is observed for the 6-nm diameter corral. For the 10-nm diameter corral a circular orbit with high LDOS occurs away from the center while the LDOS at the center is reversed and appears as dark. Further enlarging the corral to 14-nm diameter, high LDOS is observed both at the center and along a circular ring away from the center. In addition, separated spots with high LDOS also appear outside the quantum corrals for all three corrals, forming concentric circles, as marked by yellow dash lines. This suggests that the quantum confinement has meaning both inside and outside the corrals.

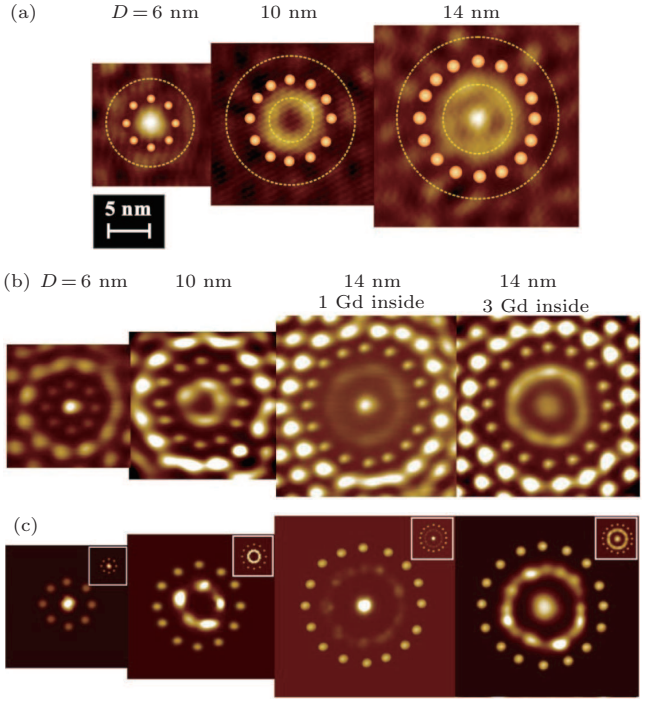

Fig. 14. (a) Experimentally obtained evolution of LDOS near E_F within the corrals. The diameters of Fe corrals (indicated by small balls for clarity) are 6, 10, and 14 nm (from left to right), respectively. Yellow dash lines indicate the position of circular high LDOS inside and outside. (b) Experimental probability distribution of Gd adatoms within circular corrals with diameters of 6, 10, 14 nm (1-Gd situation) and 14 nm (3-Gd situation) obtained by averaging hundreds of consecutive images, respectively. (c) Adatom probability distribution of KMC simulations with real positions of corral with 10^8 samplings of corresponding sizes. Inset: KMC simulations for ideal corrals of respective sizes.[94]

Gd adatoms were further deposited onto the prepatterned Ag(111) surface to study different adatom diffusion behaviors in different corrals. The statistical results of visiting probability for Gd adatoms are shown in Fig. 14(b). The Gd adatom in the 6-nm corral preferred to stay in the central area, similar to the findings for the 2D self-assembled networks with 4- or 5-nm cavities.[95,96] When the diameter of the corral was enlarged to 10 nm, the Gd adatoms diffused in a circular orbit away from the center. Both a dot orbit at the center and a circular one away from the center were observed for Gd adatoms in the 14-nm corral. To explore the role of Gd–Gd interaction when more than one orbit exists, we further studied the situation for 3 Gd adatoms diffusing inside the 14-nm corral. The differences between the 3-Gd and 1-Gd situation is that the relative probability of the two orbits has apparently changed and the orbit at the center seems to be larger in 3-Gd situation induced by the Gd–Gd LRI.[94] Apparently, these regions with high visiting probability are very close to the regions with a high LDOS, as shown in Fig. 14(a). KMC simulations were also performed with the Gd–Gd and Fe–Gd LRI. The simulated results of perfect circles show circular uniform orbit inside the corrals which are slightly different from the experiments (inset of Fig. 14(c)). This is due to the Fe adatoms in the experiments not being positioned in a perfect circle, but sometimes having 0.1–0.2 nm deviations in some directions. When we input real positions of each Fe adatom into the KMC without changing other parameters, similar features in the adatom probability distribution were reproduced (Fig. 14(c)). Our study demonstrates that one can engineer adatom motion by controlling the size of the quantum corrals.

From the above diffusion study, we learned that the orbit nearest to the Fe corral has the maximum occupancy for the Gd adatoms' visits. With increasing Gd dosage, it would be expected that most of the Gd adatoms would be located near the quantum corral, forming a ring-like structure. Indeed, the experimental data (see Fig. 15(a)) nicely demonstrated this effect. Similar findings can be obtained with KMC simulations when the experimental conditions are imposed. The result is shown in Fig. 15(b) and it is in good agreement with the experimental results. This demonstrates the possibility to use quantum confinement to create novel atomic structures.

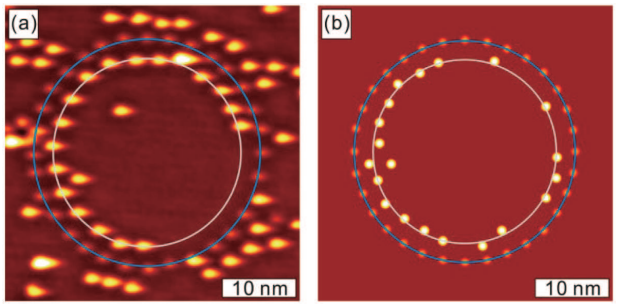

Fig. 15. (a) Typical topography image of 20 Gd atoms inside an Fe circular corral. (b) KMC simulation of the same coverage.[93] For clarity, blue and white circles indicate the Fe corral and orbits of Gd adatoms, respectively.

5. Summary

We reviewed the recent progress in both the experimental and theoretical studies of self-assembly of magnetic adatoms on noble metal surfaces, including 2D superlattices, 1D atomic strings and the novel structures formed by quantum-guiding. The formation mechanism and the empirical preconditions for the formation of a good-quality superlattice are discussed.

These novel self-assembled structures show interesting electronic properties, as revealed by scanning tunneling spectroscopy and tight-binding calculations. Besides, it is found that these self-assembled structures and adatom diffusion can be significantly modified by introducing the quantum confinement of nano-size corrals. Since these corrals can also be built by advanced lithography, further combining them with quantum engineering will open new possibilities for local functionality design down to atomic scale. Besides, in this review, we mainly focused on the discussion of the structure and electronic properties of these novel magnetic atomic structures. As these systems are magnetic, it would be even more interesting to further investigate their magnetic properties. This could be done in conjunction with high-sensitivity, high-resolution magnetic characterization tools such as spin polarized scanning tunneling microscopy.[97–100] Moreover, we touched on only a few aspects of the quantum size effect. More novel effects are expected to emerge with further exploration. In particular, the influence of the quantum size effect on the magnetic properties is still an open field to explore.

References

[1] Bader S D and Parkin S S P 2010 *Annu. Rev. Cond. Matter Phys.* **1** 71
[2] Sun S, Murray C B, Weller D, Folks L and Moser A 2000 *Science* **287** 1989
[3] Gambardella P, Dallmeyer A, Maiti K, Malagoli M C, Eberhardt W, Kern K and Carbone C 2002 *Nature* **416** 301
[4] Gambardella P, Dallmeyer A, Maiti K, Malagoli M C, Rusponi S, Ohresser P, Eberhardt W, Carbone C and Kern K 2004 *Phys. Rev. Lett.* **93** 077203
[5] Fruchart O, Klaua M, Barthel J and Kirschner J 1999 *Phys. Rev. Lett.* **83** 2769
[6] Elmers H J, Hauschild J, Höche H, Gradmann U, Bethge H, Heuer D and Köhler U 1994 *Phys. Rev. Lett.* **73** 898
[7] Shen J, Skomski R, Klaua M, Jenniches H, Manoharan S S and Kirschner J 1997 *Phys. Rev. B* **56** 2340
[8] Knorr N, Brune H, Epple M, Hirstein A, Schneider M A and Kern K 2002 *Phys. Rev. B* **65** 115420
[9] Silly F, Pivetta M, Ternes M, Patthey F, Pelz J P and Schneider W D 2004 *Phys. Rev. Lett.* **92** 016101
[10] Silly F, Pivetta M, Ternes M, Patthey F, Pelz J P and Schneider W D 2004 *New J. Phys.* **6** 16
[11] Stepanyuk V S, Klavsyuk A N, Niebergall L and Bruno P 2005 *Phys. Rev. B* **72** 153407
[12] Brovko O O, Ignatiev P A, Stepanyuk V S and Bruno P 2008 *Phys. Rev. Lett.* **101** 036809
[13] Smirnov A S, Negulyaev N N, Hergert W, Saletsky A M and Stepanyuk V S 2009 *New J. Phys.* **11** 063004
[14] Ignatiev P A, Negulyaev N N, Niebergall L, Hashemi H, Hergert W and Stepanyuk V S 2010 *Phys. Stat. Sol. (b)* **247** 2537
[15] Hashemi H, Hergert W and Stepanyuk V S 2010 *Phys. Rev. B* **81** 104418
[16] Eigler D M and Schweizer E K 1990 *Nature* **344** 524
[17] Crommie M F, Lutz C P and Eigler D M 1993 *Science* **262** 218
[18] Manoharan H C, Lutz C P and Eigler D M 2000 *Nature* **403** 512
[19] Braun K F and Rieder K H 2002 *Phys. Rev. Lett.* **88** 096801
[20] Nilius N, Wallis T M and Ho W 2002 *Science* **297** 1853
[21] Wallis T M, Nilius N and Ho W 2002 *Phys. Rev. Lett.* **89** 236802
[22] Hla S W, Braun K F and Rieder K H 2003 *Phys. Rev. B* **67** 201402(R)
[23] Fölsch S, Hyldgaard P, Koch R and Ploog K H 2004 *Phys. Rev. Lett.* **92** 056803
[24] Hirjibehedin C F, Lutz C P and Heinrich A J 2006 *Science* **312** 1021
[25] Lagoute J, Liu X and Fölsch S 2006 *Phys. Rev. B* **74** 125410
[26] Lagoute J, Nacci C and Fölsch S 2007 *Phys. Rev. Lett.* **98** 146804
[27] Wahl P, Simon P, Diekhoener L, Stepanyuk V S, Bruno P, Schneider M A and Kern K 2007 *Phys. Rev. Lett.* **98** 056601
[28] Khajetoorians A A, Wiebe J, Chilian B and Wiesendanger R 2011 *Science* **332** 1062
[29] Gomes K K, Mar W, Ko W, Guinea F and Manoharan H C 2012 *Nature* **483** 306
[30] Loth S, Baumann S, Lutz C P, Eigler D M and Heinrich A J 2012 *Science* **335** 196
[31] Chambliss D D, Wilson R J and Chiang S 1991 *Phys. Rev. Lett.* **66** 1721
[32] Brune H, Giovannini M, Bromann K and Kern K 1998 *Nature* **394** 451
[33] Whitesides G M and Grzybowski B 2002 *Science* **295** 2418
[34] Nilius N, Rienks E D L, Rust H P and Freund H J 2005 *Phys. Rev. Lett.* **95** 066101
[35] Röder H, Hahn E, Brune H, Bucher J-P and Kern K 1993 *Nature* **366** 141
[36] Gambardella P, Blanc M, Bürgi L, Kuhnke K and Kern K 2000 *Surf. Sci.* **449** 93
[37] Gambardella P, Blanc M, Brune H, Kuhnke K and Kern K 2000 *Phys. Rev. B* **61** 2254
[38] Pennec Y, Auwärter W, Schiffrin A, Weber-Bargioni A, Riemann A and Barth J V 2007 *Nat. Nano* **2** 99
[39] Ma X D, Bazhanov D I, Fruchart O, Yildiz F, Yokoyama T, Przybylski M, Stepanyuk V S, Hergert W and Kirschner J 2009 *Phys. Rev. Lett.* **102** 205503
[40] Barth J V, Costantini G and Kern K 2005 *Nature* **437** 671
[41] Repp J, Moresco F, Meyer G, Rieder K H, Hyldgaard P and Persson M 2000 *Phys. Rev. Lett.* **85** 2981
[42] Koutecký J 1958 *Trans. Faraday Soc.* **54** 1038
[43] Grimley T B 1967 *Proc. Phys. Soc.* **90** 751
[44] Einstein T L and Schrieffer J R 1973 *Phys. Rev. B* **7** 3629
[45] Lau K H and Kohn W 1978 *Surf. Sci.* **75** 69
[46] Tsong T T 1972 *Phys. Rev. B* **6** 417
[47] Tsong T T 1973 *Phys. Rev. Lett.* **31** 1207
[48] Hyldgaard P and Persson M 2000 *J. Phys.: Condens. Matter* **12** L13
[49] Negulyaev N N, Stepanyuk V S, Niebergall L, Bruno P, Pivetta M, Ternes M, Patthey F and Schneider W D 2009 *Phys. Rev. Lett.* **102** 246102
[50] Negulyaev N N, Stepanyuk V S, Niebergall L, Hergert W, Fangohr H and Bruno P 2006 *Phys. Rev. B* **74** 035421
[51] Hu J, Teng B, Wu F and Fang Y 2008 *New J. Phys.* **10** 023033
[52] Crain J N and Pierce D T 2005 *Science* **307** 703
[53] Menzel M, Mokrousov Y, Wieser R, Bickel J E, Vedmedenko E, Blügel S, Heinze S, von Bergmann K, Kubetzka A and Wiesendanger R 2012 *Phys. Rev. Lett.* **108** 197204
[54] Bose S 2003 *Phys. Rev. Lett.* **91** 207901
[55] Avellino M, Fisher A J and Bose S 2006 *Phys. Rev. A* **74** 012321
[56] Hartmann M J, Reuter M E and Plenio M B 2006 *New J. Phys.* **8** 94
[57] Hyldgaard P and Einstein T L 2003 *Appl. Surf. Sci.* **212** 856
[58] Hyldgaard P and Einstein T L 2005 *J. Cryst. Growth* **275** e1637
[59] Stepanyuk V S, Negulyaev N N, Niebergall L, Longo R C and Bruno P 2006 *Phys. Rev. Lett.* **97** 186403
[60] Ma L Y, Tang L, Guan Z L, He K, An K, Ma X C, Jia J F, Xue Q K, Han Y, Huang S and Liu F 2006 *Phys. Rev. Lett.* **97** 266102
[61] Negulyaev N N, Stepanyuk V S, Niebergall L, Bruno P, Hergert W, Repp J, Rieder K H and Meyer G 2008 *Phys. Rev. Lett.* **101** 226601
[62] Hinch B J, Koziol C, Toennies J P and Zhang G 1989 *Europhys. Lett.* **10** 341
[63] Smith A R, Chao K J, Niu Q and Shih C K 1996 *Science* **273** 226
[64] Gavioli L, Kimberlin K R, Tringides M C, Wendelken J F and Zhang Z 1999 *Phys. Rev. Lett.* **82** 129
[65] Yeh V, Berbil-Bautista L, Wang C Z, Ho K M and Tringides M C 2000 *Phys. Rev. Lett.* **85** 5158
[66] Luh D A, Miller T, Paggel J J, Chou M Y and Chiang T C 2001 *Science* **292** 1131
[67] Özer M M, Jia Y, Wu B, Zhang Z and Weitering H H 2005 *Phys. Rev. B* **72** 113409

[68] Zhang Z, Niu Q and Shih C K 1998 *Phys. Rev. Lett.* **80** 5381

[69] Hache F, Ricard D and Flytzanis C 1986 *J. Opt. Soc. Am. B* **3** 1647

[70] Liu F, Khanna S N and Jena P 1990 *Phys. Rev. B* **42** 976

[71] Qiu Z Q, Pearson J, Berger A and Bader S D 1992 *Phys. Rev. Lett.* **68** 1398

[72] Li J, Przybylski M, Yildiz F, Ma X D and Wu Y Z 2009 *Phys. Rev. Lett.* **102** 207206

[73] Lang N D and Avouris P 1998 *Phys. Rev. Lett.* **81** 3515

[74] Guo Y, Zhang Y F, Bao X Y, Han T Z, Tang Z, Zhang L X, Zhu W G, Wang E G, Niu Q, Qiu Z Q, Jia J F, Zhao Z X and Xue Q K 2004 *Science* **306** 1915

[75] Li J, Schneider W D, Berndt R and Crampin S 1998 *Phys. Rev. Lett.* **80** 3332

[76] Niebergall L, Rodary G, Ding H F, Sander D, Stepanyuk V S, Bruno P and Kirschner J 2006 *Phys. Rev. B* **74** 195436

[77] Pietzsch O, Okatov S, Kubetzka A, Bode M, Heinze S, Lichtenstein A and Wiesendanger R 2006 *Phys. Rev. Lett.* **96** 237203

[78] Oka H, Ignatiev P A, Wedekind S, Rodary G, Niebergall L, Stepanyuk V S, Sander D and Kirschner J 2010 *Science* **327** 843

[79] Ding H F, Pearson J E, Li D, Cheng R, Fradin F Y and Bader S D 2005 *Rev. Sci. Instru.* **76** 123703

[80] Zhang X P, Miao B F, Sun L, Gao C L, Hu A, Ding H F and Kirschner J 2010 *Phys. Rev. B* **81** 125438

[81] Negulyaev N N, Stepanyuk V S, Niebergall L, Bruno P, Auwarter W, Pennec Y, Jahnz G and Barth J V 2009 *Phys. Rev. B* **79** 195411

[82] Stepanyuk V S, Niebergall L, Longo R C, Hergert W and Bruno P 2004 *Phys. Rev. B* **70** 075414

[83] Fichthorn K A and Weinberg W H 1992 *Phys. Rev. Lett.* **68** 604

[84] Fichthorn K A and Scheffler M 2000 *Phys. Rev. Lett.* **84** 5371

[85] Brune H 1998 *Surf. Sci. Rep.* **31** 125

[86] Cao R X, Zhang X P, Miao B F, Zhong Z F, Sun L, You B, Hu A and Ding H F 2013 *Surf. Sci.* **610** 65

[87] Ternes M, Weber C, Pivetta M, Patthey F, Pelz J P, Giamarchi T, Mila F and Schneider W D 2004 *Phys. Rev. Lett.* **93** 146805

[88] Li J, Schneider W D and Berndt R 1997 *Phys. Rev. B* **56** 7656

[89] Ding H F, Stepanyuk V S, Ignatiev P A, Negulyaev N N, Niebergall L, Wasniowska M, Gao C L, Bruno P and Kirschner J 2007 *Phys. Rev. B* **76** 033409

[90] Smoluchowski R 1941 *Phys. Rev.* **60** 661

[91] Cao R X, Zhong Z F, Hu J, Zhang X P, Miao B F, Sun L, You B, Wu D, Hu A, Zhang W Y and Ding H F 2013 *Appl. Phys. Lett.* **103** 081608

[92] Schiffrin A, Reichert J, Auwärter W, Jahnz G, Pennec Y, Weber-Bargioni A, Stepanyuk V S, Niebergall L, Bruno P and Barth J V 2008 *Phys. Rev. B* **78** 035424

[93] Cao R X, Miao B F, Zhong Z F, Sun L, You B, Zhang W, Wu D, Hu A, Bader S D and Ding H F 2013 *Phys. Rev. B* **87** 085415

[94] Hu J, Cao R X, Miao B F, Liu Z, Zhong Z F, Sun L, You B, Wu D, Zhang W, Hu A, Bader S D and Ding H F 2013 *Surf. Sci.* **618** 148

[95] Cheng Z, Wyrick J, Luo M, Sun D, Kim D, Zhu Y, Lu W, Kim K, Einstein T L and Bartels L 2010 *Phys. Rev. Lett.* **105** 066104

[96] Pivetta M, Pacchioni G E, Schlickum U, Barth J V and Brune H 2013 *Phys. Rev. Lett.* **110** 086102

[97] Bode M, Getzlaff M and Wiesendanger R 1998 *Phys. Rev. Lett.* **81** 4256

[98] Wulfhekel W and Kirschner J 1999 *Appl. Phys. Lett.* **75** 1944

[99] Ding H F, Wulfhekel W and Kirschner J 2002 *Europhys. Lett.* **57** 100

[100] Bode M 2003 *Rep. Prog. Phys.* **66** 523